Original article

Solid and liquid state characterization of tetrahydrocurcumin using XRPD, FT-IR, DSC, TGA, LC-MS, GC-MS, and NMR and its biological activities

Mahendra Kumar Trivedi [a], Parthasarathi Panda [b], Kalyan Kumar Sethi [b], Mayank Gangwar [b], Sambhu Charan Mondal [b], Snehasis Jana [b, *]

[a] *Trivedi Global Inc., Henderson, 89052, Nevada, USA*
[b] *Trivedi Science Research Laboratory Pvt. Ltd., Thane, (W)-400604, Maharashtra, India*

A B S T R A C T

Tetrahydrocurcumin (THC) is one of the major metabolites of curcumin (CUR), an ancient bioactive natural polyphenolic compound. This research article describes both the solid and liquid state characterization of THC using advanced spectroscopic and thermo-analytical techniques. Anti-inflammatory, anti-oxidant, and neuroprotective activities of THC were investigated using *in vitro* cell lines. Liquid chromatography-mass spectrometry analysis revealed that our sample comprised 95.15% THC, 0.51% tetrahydrodemethoxycurcumin (THDC), 3.40% hexahydrocurcumin, and 0.94% octahydrocurcumin. Gas chromatography-mass spectrometry analysis indicated the presence of 96.68% THC and 3.32% THDC. THC in solution existed as keto-enol tautomers in three different forms at different retention time, but the enol form was found to be dominant, which was also supported by nuclear magnetic resonance analysis. THC was thermally stable up to 335.55 °C. THC exhibited more suppression of cytokines (TNF-α, IL-1β, and MIP-1α) than CUR in a concentration-dependent manner in mouse splenocytes, while NK-cell and phagocytosis activity was increased in macrophages. THC showed a significant reduction of free radicals (LPO) along with improved antioxidant enzymes (SOD and catalase) and increased free radical scavenging activity against ABTS$^+$ radicals in HepG2 cells. THC displayed higher protection capability than CUR from oxidative stress and neuronal damage by improving cell viability against H_2O_2 induced HepG2 cells and MPP$^+$ induced SH-SY5Y cells, respectively, in a concentration-dependent manner. Thus, a variation of the biological activities of THC might rely on its keto-enol form and the presence of other THC analogs as impurities. The present study could be advantageous for further research on THC for better understanding its physicochemical properties and biological variation.

1. Introduction

Since the beginning of human civilization, natural products have been popularly used for medicines, food, and spices based on their tremendous biological activities. Tetrahydrocurcumin (THC) or tetrahydrodiferuloylmethane or 1,7-bis(4-hydroxy-3-methoxyphenyl)-3,5-heptanedione (**1**, mol. formula: $C_{21}H_{24}O_6$; mol. wt. of 372.41) is the major metabolite of curcumin (CUR), a bis-α,β-unsaturated β-diketone polyphenol [1,2]. CUR belongs to diarylheptanoid classes

and is usually found as curcuminoids in the rhizome (turmeric) of *Curcuma longa* Linn (*Zingiberaceae*) with demethoxycurcumin (DMC), bis-demethoxycurcumin (BDMC), and cyclocurcumin (CC) as shown in Fig. 1 [3,4]. THC is commonly prepared from curcuminoids by hydrogenation using platinum catalysts like PtO_2 and palladium catalysts like 10% Pd/C [5,6]. Besides THC, other reductive metabolites of CUR such as dihydrocurcumin (DHC), hexahydrocurcumin (HHC) and octahydrocurcumin (OHC) (Fig. 1), tetrahydrodemethoxycurcumin (THDC), tetrahydrobisdemethoxycurcumin (THBDC), hexahydrodemethoxycurcumin, octahydrodemethoxycurcumin, hexahydrobis demethoxy-curcumin, and octahydrobisdemethoxycurcumin are found during chemical and enzymatic reactions [3,7,8].

Girija et al. reported that THC is non-planar, and its benzene rings are orthogonally located at the ends of the heptane chain with

a dihedral angle of 84.09 (7)°. They concluded that the 'heptane-3,5-dione' moiety in THC in solid state exists in the keto-enol form with the hydrogen atom of OH disordered over two adjacent sites and produces two-dimensional sheets through a strong intra-molecular hydrogen bond [5]. THC is more hydrophilic and stable in 0.1 M phosphate buffers at various pH values than CUR [9]. Literature reported that THC possesses anti-oxidant, anti-inflammatory, chemopreventive, antibacterial, antidyslipidemic, antiviral, cyto-toxic, antiangiogenic, neurological, antihistamine, immunological, and anti-aging activities [9,10]. Unlike CUR, THC is quite stable in the intestine and still retains anti-oxidant activities at neutral or basic pH. The lack of α,β-unsaturated carbonyl moiety in THC is responsible for C—C bond cleavage at the active methylene carbon of β-diketone group during oxidation, producing smaller o-methoxy phenol products which also act as an antioxidant. Therefore, THC possesses higher antioxidant activity than CUR, as claimed by some scientific studies [9]. Consequently, THC is unable to form Michael adducts with intracellular proteins, phase-II en-zymes which are responsible for histone acetyltransferases (HAT) inhibitory activity, inducing HO-1, and NF-κB suppression in cells by CUR. Thus, THC has less antitumor and anti-inflammatory ac-tivity than CUR [4,9,11]. THC can be useful in treating post-menopausal and osteoarthritis symptoms and reduces the expressions of pro-inflammatory cytokines in estrogen-deficient rats fed on a high-fat diet [10]. THC is found to be useful as a safe whitening agent, anti-aging, and skin rejuvenator in the cosmetic industry for wound healing and also for treating various skin-related disorders [12].

As THC has the almost structural similarity with CUR and con-tains the β-diketone moiety except the vinylic double bond, it can also exist in keto-enol tautomers. Consequently, the tautomers, chameleons of chemistry, have the capability to change instantly an apparently established structure to another one through a simple change of phase and back again by restoring its original condition. Various factors such as intra and intermolecular interactions, sol-vent effects, physical state, hydrogen bond formation, and tem-perature play an important role in the keto-enol equilibrium, facilitating the dominant keto or enol form. A detailed study of the keto-enol tautomerism offers to acquire knowledge of the physi-cochemical properties and biological activities of the pharmaceu-ticals/nutraceuticals in which it occurs [13,14]. To the best of our knowledge, the comprehensive investigation in physicochemical, structural, and thermal properties of THC in both solid and liquid states is not yet reported. Thus, this article was aimed to charac-terize THC in both solid and liquid states to understand its physi-cochemical and thermal properties as well as to evaluate its biological effects on pro-inflammatory cytokines, natural killer cells, phagocytosis, lipid peroxidation, oxidative stress, and neuronal damage by using different in vitro cell line models.

2. Experimental

2.1. Chemicals and materials

THC was purchased from Novel Nutrient. Pvt. Ltd., India. This commercially purchased THC, which was prepared from *Curcuma longa,* was claimed to contain 95.51% tetrahydrocucuminoids. Thus, the present sample used for both characterization and biological activities is actually tetrahydrocucuminoids. However, THC was used to represent our sample for comparing with the literature. CUR (99% purity) was purchased from Qualikems Fine Chemicals Pvt. Ltd., India. The HPLC grade acetonitrile, methanol, and formic acid were purchased from Merck, USA. Milli Q® water was procured from Merck Millipore, USA. All the other chemicals used in this experiment were of analytical grade procured from local vendors.

2.2. Characterization of THC

2.2.1. Liquid chromatography-mass spectrometry (LC-MS) analysis

The LC-MS analysis of THC was carried out on LC-Dionex Ulti-mate 3000, MS-TSQ Endura, USA, equipped with a binary pump, autosampler, column heater, a photo-diode array (PDA) detector connected with a triple-stage quadrupole mass spectrometer (Thermo Scientific TSQ Endura, USA) equipped with a Thermo Scientific Ion Max NG source and heated electrospray ionization probe. The column used here was a reversed phase Zorbax SB-C$_{18}$
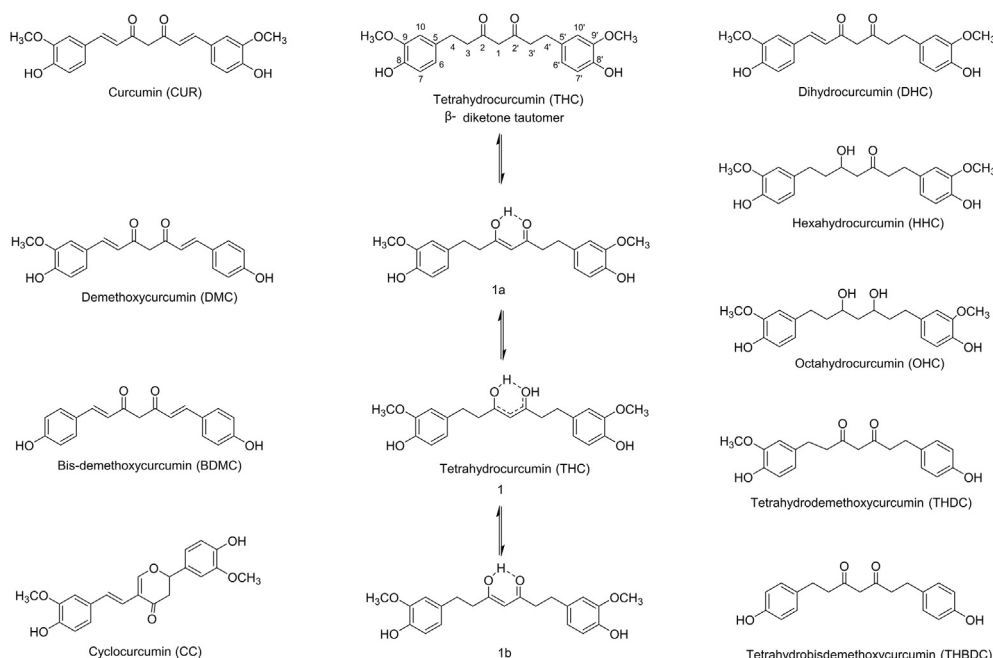

Fig. 1. Curcuminoids isolated from the rhizomes of *Curcuma longa* and their reductive metabolites.

(100 mm × 4.6 mm, 3.5 μm), maintained at 40 °C. 10 μL of THC solution in methanol was injected, and the analyte was eluted using 2 mM ammonium formate in water with 0.5% formic acid (mobile phase A), and acetonitrile (mobile phase B) pumped at a constant flow rate of 0.6 mL/min. Chromatographic separation was achieved using isocratic gradient program as follow: 0.1 min-5%B; 5.0 min-5%B; 15.0 min-75%B; 20.0 min-75%B; 25.0 min-95%B; 30.0 min-95%B; 35.0 min-5%B and 40.0 min-5% B and the total run time was 40 min. Peaks were monitored at 280 nm using the PDA detector. The mass spectrometric analysis was performed under positive ESI mode with the following operational parameters: sheath gas 52 Arb; aux gas 16 Arb; ion transfer tube 356 °C; vaporizer temperature 420 °C [15]. The total ion chromatogram, peak area (%), and mass spectrum of the individual peak, which appeared in LC along with the full scan (m/z 50–1500), were recorded.

2.2.2. Gas chromatography-mass spectrometry (GC-MS) analysis

An Agilent 7890B gas chromatograph equipped with a 30 m × 0.25 mm i.d., silica capillary column (HP-5 MS) and coupled to a quadrupole detector with pre-filter (5977B, USA) was operated with electron impact (EI) ionization in positive/negative mode at 70 eV. Oven temperature was programmed from 50 °C (1 min hold) to 150 °C at 20 °C/min to 200 °C (6 min hold) at 25 °C/min (12 min hold). Temperatures of the injector, detector (FID), auxiliary, ion source, and quadrupole detector were 230, 250, 280, 230, and 150 °C. Sample (5.0 μL) dissolved in methanol was splitlessly injected with helium as carrier gas with a flow rate of 2.0 mL/min. Mass spectra were scanned from m/z 40 to 1050 at stability of ±0.1 m/z mass accuracy over 48 h [15]. The identification of analyte was done by GC retention time and by a comparison of the mass spectra of identified substances with those of authentic reference substances.

2.2.3. Fourier transform infrared (FT-IR) spectroscopy

The FT-IR spectrum of THC was recorded on spectrum ES (PerkinElmer, USA) FT-IR spectrometer with the frequency range of 400–4000 cm^{-1} at a resolution of 4 by mixing THC with potassium bromide (KBr) [16].

2.2.4. Nuclear magnetic resonance (NMR) analysis

^{1}H and ^{13}C NMR analyses of THC by dissolving in DMSO-d_6 were conducted at 400 MHz and 100 MHz, respectively, on an Agilent-MRDD2 FT-NMR spectrometer at room temperature using TMS as an internal standard. ^{1}H NMR multiplicities were designated as singlet (s), doublet (d), triplet (t), multiplet (m), and broad (br). Chemical shifts (δ) were in parts per million (ppm) relative to the solvent's residual proton chemical shift (DMSO-d_6, δ = 2.50 ppm) and the solvent's residual carbon chemical shift (DMSO-d_6, δ = 39.52 ppm) [15].

2.2.5. Ultraviolet−visible (UV−Vis) spectroscopy analysis

The UV−Vis spectral analysis of THC was performed using a Shimadzu UV-2400PC SERIES with UV Probe, Japan, using 1 cm quartz cell that has a slit width of 0.5 nm. The wavelength range used for recording the spectrum was 190–800 nm [16].

2.2.6. X-ray powder diffraction analysis (XRPD)

The crystalline state of THC in solid state (powder form) was estimated by a PANalytical X'PERT3 powder X-ray diffractometer, UK. The diffraction of the analyte was carried out using a copper line as the source of radiation at the X-ray of the wavelength of 0.154 nm, running at 45 kV voltage and 40 mA current with a scanning rate of 18.87°/s over a 2θ range of 3–90°. The ratio of Kα-2 and Kα-1 in this instrument was 0.5 (k, equipment constant).

The data were collected in the form of a chart of the Bragg angle (2θ) vs. intensity (counts per second), and a detailed table containing information on peak intensity counts, d value (Å), relative intensity (%), full width half maximum (FWHM) (°2θ), area (cts*°2θ) using X'pert data collector and X'pert high score plus processing software [16].

2.2.7. Particle size analysis (PSA)

The PSA of THC was performed on Malvern Mastersizer 3000, UK, with a detection range between 0.01 μm and 3000 μm using the wet method. The sample unit (Hydro MV) was filled with a dispersant medium (light liquid paraffin oil) and the stirrer was operated at 2500 rpm. The refractive index values for dispersant and samples were 0.0 and 1.47. The measurement was taken twice after reaching obscuration between 10% and 20%, and the average was taken of two measurements. Consequently, PSA of THC was repeated for three times to obtain the average particle size distribution. d(0.1) μm, d(0.5) μm, d(0.9) μm represent particle diameter corresponding to 10%, 50%, and 90% of the cumulative distribution. D(4,3) represents the average mass-volume diameter, and SSA is the specific surface area (m^2/kg). The calculations were done by using software Mastersizer V3.50 [16].

2.2.8. Differential scanning calorimetry (DSC) analysis

The DSC thermogram of THC was achieved in a DSC Q2000 differential scanning calorimeter, USA, under a dynamic nitrogen atmosphere with a flow rate of 50 mL/min with a sample mass of 2.72 mg using aluminum pan at a heating rate of 10 °C/min from 30 °C to 400 °C [16].

2.2.9. Thermal gravimetric analysis (TGA)/differential thermogravimetric analysis (DTG)

TGA/DTG thermograms of THC were obtained in a TGA Q500 thermoanalyzer apparatus, USA, under dynamic nitrogen atmosphere (50 mL/min) using a platinum crucible at a heating rate of 10 °C/min from 25 °C to 900 °C with a sample mass of 5.56 mg [16].

2.3. Biological activities of THC

2.3.1. Cell lines and culture

HepG2 cell line (hepatocellular carcinoma), mouse lymphoma cell line (Yac-1), macrophage and SH-SY5Y neuroblastoma cells were procured from National Centre for Cell Science, India. Mouse spleen was used for the isolation of splenocyte as per the standard protocol [17]. HepG2 and SH-SY5Y neuroblastoma cells were cultured in EMEM containing 10% FBS, trypsin (0.2%) and EDTA (0.02%) under the growth condition of 37 °C, 95% humidity, and 5% CO$_2$. For splenocyte maintenance, lipopolysaccharide (LPS) (0.5 μg/mL) induced splenocyte cultures were grown for 48 h at 37 °C in a humidified CO$_2$ incubator (5% CO$_2$) [18]. The single cell suspension of splenocytes co-incubated with mouse lymphoma cell line (Yac-1) for the estimation of natural killer (NK) cells activity in RPMI medium containing 10% FBS was plated at a density of 2×10^4 cells per well in 96-well culture plates. The LPS (0.5 μg/mL) induced splenocyte cultures were grown for 24 h at 37 °C in a humidified CO$_2$ incubator (5% CO$_2$). The macrophages (5×10^4 cells per well) were grown in 24-well culture plates using RPMI-1640 medium supplemented with 10% FBS, 100 μg/mL of streptomycin, and 100 units/mL of penicillin for phagocytosis activity. The LPS (0.5 μg/mL) induced macrophage cultures were grown as per the Yac-1 culture condition (RPMI 1640 with 2 mM ʟ-glutamine and 10% FBS). The respective vehicle control kept in the assay was DMSO with LPS.

2.3.2. MTT assay

Cytotoxicity was determined by exposing cells to different

concentrations of THC and CUR. The concentrations were selected based on the literature and *in vitro* cells viability assay as per in house preliminary studies. The respective vehicle control kept in the assay was DMSO with LPS. The number of viable cells was estimated based on the conversion of MTT to formazan dye using a mitochondrial enzyme. The effect of the THC and CUR on cell viability was determined with the help of the following equation (1):

$$\% \text{ Cell viability} = (100 - \% \text{ cytotoxicity}) \qquad (1)$$

Where % Cytotoxicity = {(O.D. of Control cells − O.D. of cells treated with THC/CUR)/OD of control cells}*100 [19].

2.3.3. Cytokines assay

Cytokines assays for TNF-α, IL-1β, and MIP-1α were performed by ELISA method in culture supernatants using a Biotek reader (SIAFRT/Synergy HT multimode reader). For the estimation of important cytokines, LPS (0.5 μg/mL) induced splenocytes were exposed to the THC and CUR at selected non-toxic concentration. After 48 h of incubation, supernatants were analyzed for the secreted levels of cytokines as per the manufacturer's instructions [20].

2.3.4. Natural killer (NK) cells assay

NK cell activity was performed in culture supernatants (mouse splenocytes) by ELISA method using Biotek reader (SIAFRT/Synergy HT multimode reader) according to the method described in the literature [21]. The resultant NK cells activity in the presence of LPS was determined with the help of the following equation (2):

% NK cells activity = [(OD of Yac-1 cells alone) - {(OD of NK + Yac-1 cells) - (NK alone)}]/OD of Yac-1 cells alone]*100   (2)

2.3.5. Phagocytosis assay

The effects of THC and CUR on phagocytosis assay were measured in culture supernatants using CytoSelect™ 96-Well Phagocytosis Assay kit (Zymosan, Colorimetric Format) as per the manufacturer's instructions (Cell Biolabs Inc. USA). This assay was made using the quantitative colorimetric detection of engulfed pre-labeled zymosan particles by mouse macrophages cell line (RAW264.7). For the estimation of the extent of phagocytosis in LPS (0.5 μg/mL) induced macrophage, the cells were exposed to THC and CUR at selected non-toxic concentrations. After 24 h of incubation, supernatants were analyzed to assess the extent of phagocytosis colorimetrically as per the manufacturer's instructions [22]. The resultant modulatory effect of THC/CUR-mediated phagocytosis in the presence of LPS was determined by the following equation (3):

% Increase in phagocytosis = [{O.D at 405 nm in LPS + THC/CUR treated cells − O.D. at 405 nm in LPS treated control cells}] / O.D. at 405 nm in LPS treated control cells]*100   (3)

2.3.6. Antioxidant potential of THC

Antioxidant capacity was determined using estimation of free radical, LPO (lipid peroxidation), and antioxidant enzymes *viz.* superoxide dismutase (SOD) and catalase (CAT), which were investigated in HepG2 cells exposed to THC and CUR (0.01, 0.1, 1, and 10 μg/mL). Cells were lysed by sonication and then centrifuged at 10,000 *g* for 30 min at 4 °C. The supernatant was used to determine the enzyme activity. Hydrogen peroxide (20 mM) was used to induce stress and denoted as vehicle control in the estimation of LPO, SOD, and CAT. However, the total antioxidant capacity of THC

and CUR was also determined using ABTS radical scavenging assay using the method described by Re et al. [23].

2.3.7. Anti-oxidative damage and neuroprotective effects of THC on MPP^+ induced apoptotic cell death in SH-SY5Y neuroblastoma cells

Scavenging activity of hydrogen peroxide by THC and CUR was estimated using the modified literature method, which defined the THC and CUR protection against oxidative damage by hydrogen peroxide (H_2O_2) in HepG2 cells [24]. However, the neuroprotective effects of THC and CUR were determined in SH-SY5Y neuroblastoma cells. The cell viability in HepG2 and SH-SY5Y neuroblastoma cells was analyzed using MTT assay. Briefly, 24 h following treatment with the various concentrations of MPP^+ (1-methyl-4-phenylpyridinium), cells in the 96-well plates were washed with phosphate-buffered saline, after which the cells were incubated with MTT (5 mg/mL) at 37 °C for 4 h. Subsequently, the supernatants were removed, 100 μL of dimethyl sulfoxide was added to each well, and the plates were agitated on a microplate shaker in order to dissolve the blue MTT-formazan. Absorbance was measured at 570 nm using an ELx800 microplate reader (BioTek Instruments, Inc., Winooski, VT, USA). Cell viability was expressed as the ratio of the signal obtained from the treated cultures to the control cultures [25].

2.3.8. Statistical analysis

Data were expressed as mean ± SD, and represented the mean of three independent experiments ($n = 3$). Data were tested using a one-way analysis of variance (ANOVA), followed by post-hoc analysis by Tukey's test for multiple comparisons. The statistical data were represented as significant *F* test and the significance was considered at $P \leq 0.05$.

3. Results

The commercially purchased THC, which was claimed to contain 95.51% tetrahydrocurcuminoids, was characterized thoroughly using LC-MS, GC-MS, FT-IR, NMR, UV–Vis spectroscopy, XRD, PSA, DSC, and TGA to understand its structural, physicochemical and thermal properties. Consequently, this sample was used for in vitro studies on different cell lines.

3.1. Structural characterization of THC

The liquid chromatogram of the analyte (Fig. 2A) shows the presence of six peaks, among which 4 peaks were sharp with higher % area at the retention time of 15.20, 16.08, 17.31 and 17.48 min, while the two small peaks had the retention time at 14.66 and 15.89 min.

Compounds **1–6** were proposed through the molecular ion peak along with the ESI mass spectra of THC at the retention time of 14.66, 15.20, 15.89, 16.08, 17.31, and 17.48 min (Figs. S1–S6). OHC exhibited the mass of the protonated molecular ion at *m/z* 380.38 $[M + 4H]^+$ (calculated for $C_{21}H_{32}O_6{}^{4+}$, 380.22) with the fragment ion peak (base peak) at *m/z* 341.76 which corresponds to the molecular formula $C_{21}H_{26}O_4{}^{2+}$ at the retention time of 14.66 min (Fig. S1). The ESI-mass spectrum at the retention time of 15.20 min (Fig. S2) revealed the presence of the molecular mass of HHC at *m/z* 396.65 $[M + Na]^+$ (calculated for $C_{21}H_{26}O_6Na^+$, 397.17). The characteristic fragment ion peaks at *m/z* 357.97, 340.35, 260.11, 177.02, 163.13, and 136.96, which correspond to the molecular formula $C_{21}H_{24}O_4{}^{2+}$, $C_{19}H_{16}O^{\bullet\bullet2+}$, $C_{11}H_{13}O_2{}^+$, $C_{11}H_{15}O^+$, and $C_9H_{12}O^+$, supported the structure of HHC. Consequently, THDC exhibited the protonated mass at *m/z* 343.36 (calculated for $C_{20}H_{23}O_5{}^+$, 343.15) with the major fragment ion peak (base peak) at *m/z* 325.14 corresponding to the molecular formula $C_{20}H_{21}O_4{}^+$ at the retention

time of 15.89 min (Fig. S3). Thereafter, the ESI-mass spectra of THC at the retention time of 16.08 min (Fig. S4) exhibited the mass of THC at m/z 373.02 $[M + H]^+$ (calculated for $C_{21}H_{25}O_6^+$, 373.16) and 395.83 $[M + Na]^+$ (calculated for $C_{21}H_{24}O_6Na^+$, 395.16) along with the fragment ion peak at m/z 354.76 (base peak), 325.50, 177.03, and 137.05 which correspond to the molecular formula $C_{21}H_{23}O_5^+$, $C_{20}H_{21}O_4^+$, $C_{11}H_{13}O_2^+$, and $C_8H_9O_2^+$. Similarly, the ESI-mass spectra of THC at the retention time of 17.31 min (Fig. S5) showed the mass of THC at m/z 395.41 $[M + Na]^+$ (calculated for $C_{21}H_{24}O_6Na^+$, 395.16) along with the fragment ion peak at m/z 355.10 (base peak), 325.14, and 177.26. The ESI-mass spectra of THC at the retention time of 17.48 min (Fig. S6) also displayed the mass of THC at m/z 373.21 and 395.45 along with the fragment ion peak at m/z 356.17 (base peak), 325.32, 179.14, and 137.10 corresponding to the molecular formula $C_{21}H_{24}O_5^+$, $C_{20}H_{21}O_4^+$, $C_{11}H_{15}O_2^+$, and $C_8H_9O_2^+$. On the other hand, gas chromatogram of THC (Fig. 2B) exhibited two peaks at the retention time of 23.85 and 25.46 min. The GC mass spectrum of THC at the retention time of 23.85 min (Fig. S7) showed the molecular mass for THDC at m/z 342.1 $[M]^+$ (calculated for $C_{20}H_{22}O_5^+$, 342.1) along with the fragment ion peaks at m/z 150.1, 137.1, 122.0, 107.1, and 77.1 which correspond to the molecular formula $C_9H_{10}O_2^{+•}$, $C_8H_9O_2^+$, $C_8H_{10}O^+$, $C_7H_7O^+$, and $C_6H_5^+$, respectively. The mass spectra of THC at the retention time of 25.46 min (Fig. S8) exhibited the molecular mass for THC at m/z 372.2 $[M]^+$ (calculated for $C_{21}H_{24}O_6^+$, 372.2) along with the fragment ion peak at m/z 137.1 (base peak) corresponding to the molecular formula $C_8H_9O_2^+$. Thus, LC-MS and GC-MS analyses confirmed the presence of THDC in our analyte.

Hoehle et al. [7] reported the GC-MS analysis of THC after trimethylsilylation by dissolving THC in *N,O*-bis(trimethylsilyl) trifluoroacetamide. However, the current GC-MS analysis (Fig. 2B), which was carried out by dissolving THC in methanol, exhibited the presence of the mass of THC without derivatized THC. Consequently, our sample was thoroughly analyzed with FT-IR, NMR, and UV−Vis spectroscopy for understanding the detailed structure of THC. The FT-IR and proton NMR data of THC (Fig. 3 and Table 1) were compared with the reported value [6] and indicated the presence of keto-enol tautomerism.

The IR spectrum of THC (Fig. 3A) displayed a strong, broad absorption band for the hydroxyl group at 3426 cm^{-1}, C-H$_{sp}^2$ stretching at 3064 and 3005 cm^{-1}, and C-H$_{sp}^3$ stretching at 2962, 2935, 2845 cm^{-1}. An intense band at 1602 cm^{-1} assigned to the vibrations of the carbonyl bond (C=O) accompanied by a small shoulder at 1739 cm^{-1} was ascribed to the keto-enol tautomerism of THC. A strong, sharp vibrational band at 1515 cm^{-1} for aromatic ring stretching, 1276 cm^{-1} for enol C−O stretching, 1033 cm^{-1} for -C-O-CH$_3$ stretching, medium absorption bands at 1458 and 1371 cm^{-1} for C−H bending of the methyl groups, 1406 cm^{-1} for O−H bending, and 1116 cm^{-1} for C-OH were observed in the FT-IR spectrum of THC (Fig. 3A) supporting the structure of THC.

The ^{1}H and ^{13}C NMR spectral analysis of THC (Table 1), along with the reported data [6], revealed the structure of THC. A singlet at δ 5.72 and δ 99.63 ppm was ascribed to the one proton and carbon, respectively for the central carbon (C-1) of the β-diketone in its enol form, while singlet at δ 3.67 and δ 56.34 ppm for the proton and carbon, respectively for C-1 was attributed to its keto form. The two different carbon signals for C-2 and C-3 (Fig. S9) might be due to the keto and enol forms of THC.

The UV−Vis spectrum of THC (Fig. S10) exhibited a broad absorption maximum at 282 nm (λ$_{max}$) with a shoulder peak at
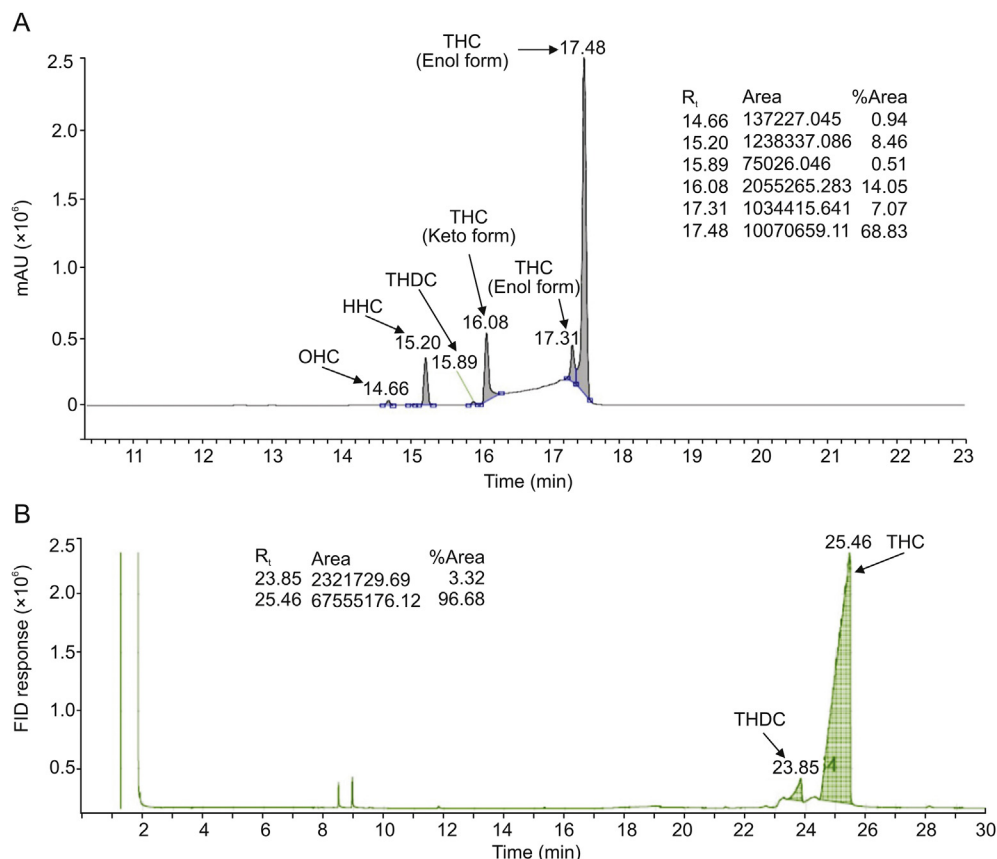

Fig. 2. (A) Liquid chromatogram and (B) gas chromatogram of THC.

~300 nm in ethanol. This type of absorption is attributed to the combination of $\pi \rightarrow \pi^*$ and $n \rightarrow \pi^*$ electronic transition in enolic form in solution [26]. The λ_{max} is nearly matched with reported value [1,7].

3.2. Physicochemical and thermal study of THC

The XRPD analysis of the analyte revealed the presence of the well-defined, narrow, sharp, and intense peaks, as shown in Fig. 4A, indicating that the commercially purchased THC is crystalline in nature. The detailed morphology of THC crystal, *i.e.,* relative intensity (%), full width half maximum (FWHM), area, and crystallite size (G, nm) of THC, is provided in Table 2. The crystallite size (G, nm) was calculated from the Scherrer equation [27] as follows:

$$G = k\lambda/(bCos\theta) \tag{4}$$

Where k is the equipment constant (0.5), λ is the X-ray wavelength (0.154 nm); b in radians is the full-width at half of the peaks, and θ is the corresponding Bragg angle.

The crystallite size was found to be in the range from 15.81 to 49.86 nm (Table 2).

The particle size analysis of THC was repeated three times, and the results are summarized in Table 3. The average particle size distribution of THC ($n = 3$) was observed at d(0.1) = 18.2 μm, d(0.5) = 56.0 μm, d(0.9) = 360.7 μm and D(4,3) = 121.9 μm. The average specific surface area (SSA) of magnesium gluconate was 164.8 m^2/kg.

The DSC thermogram of THC (Fig. 4B) exhibited the presence of a sharp endothermic inflection at 92.61 °C along with a broad endothermic peak at 348.37 °C. The peak temperature at 92.61 °C is

Table 1
^{1}H and ^{13}C NMR data of THC (400 MHz, DMSO-d_6, δ in ppm, *J* in Hz).

Position	^{1}H NMR	^{13}C NMR
1	5.72 (1H, s)[a], 3.67 (2H, s)[b]	99.63[a], 56.34[b]
2, 2	–	204.64[b], 193.39[a]
3, 3	2.70–2.75 (4H, m)	30.47, 28.41
4, 4	2.63 (2H, dd, *J* = 6.4, 7.2)[a], 2.54 (2H, dd, *J* = 7.6, 8.4)[b]	44.73
5, 5	–	131.62, 131.39
6, 6	6.55 (2H, t, *J* = 10.4)	120.30, 120.41
7, 7	6.74 (2H, d, *J* = 15.2)	115.31, 115.09
8, 8	–	147.40
9, 9	–	144.74, 144.55
10, 10	6.63 (2H, dd, *J* = 2.4, 8.4)	112.46, 112.42
-OH	8.65 (2H, d, *J* = 8.4)	–
-OCH$_3$	3.71 (6H, s)	55.51

δ: delta (chemical shift), s: singlet, br: broad, d: doublet, dd: doublet of doublet, t: triplet, and m: multiplet.
[a] Enol form.
[b] Keto form.

the melting temperature of THC with an enthalpy of fusion (ΔH_{fusion}) of 98.85 J/g. The broad endothermic peak at 348.37 °C may be the slow degradation of non-volatile intermediates, according to the literature [28]. The TGA thermogram of THC (Fig. 4C) showed no significant loss up to 200 °C. Consequently, a major rapid weight loss (96.37%) occurred up to 350 °C, which might be due to the first dehydroxylation of hydroxyl groups and subsequent degradation of non-volatile intermediates affording the formation of amorphous carbon. DTG curve shows the maximal decomposition temperature at 335.55 °C. The current TGA/DTG analysis revealed that THC was thermally stable up to 335.55 °C.
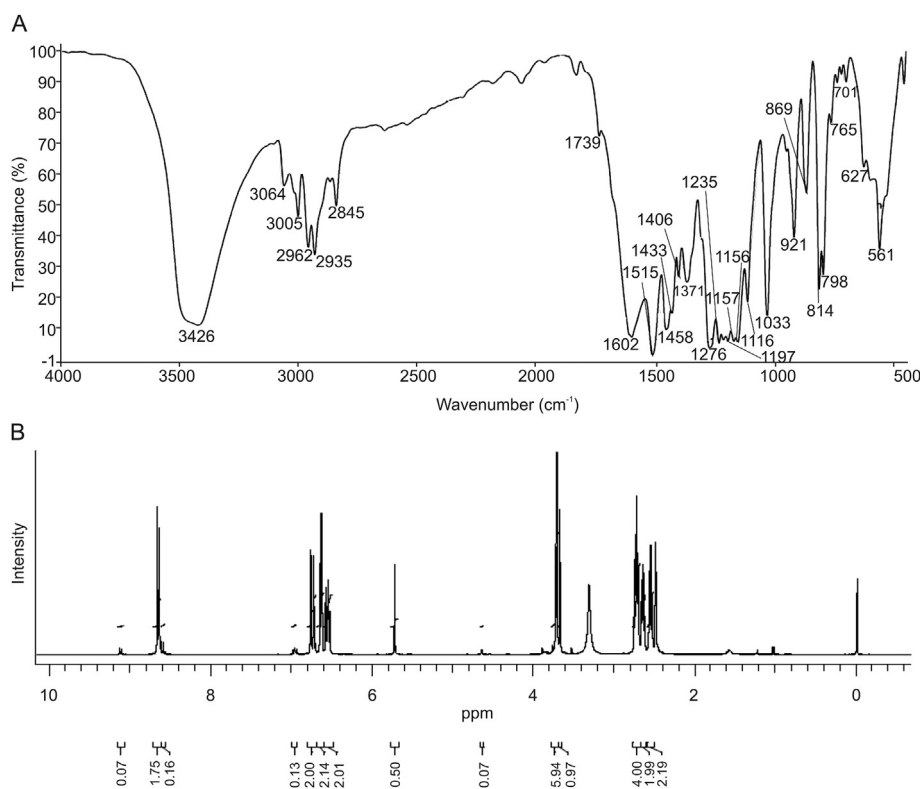

Fig. 3. (A) FT-IR spectrum and (B) ^{1}H NMR spectrum (400 MHz, DMSO-d_6) of THC.
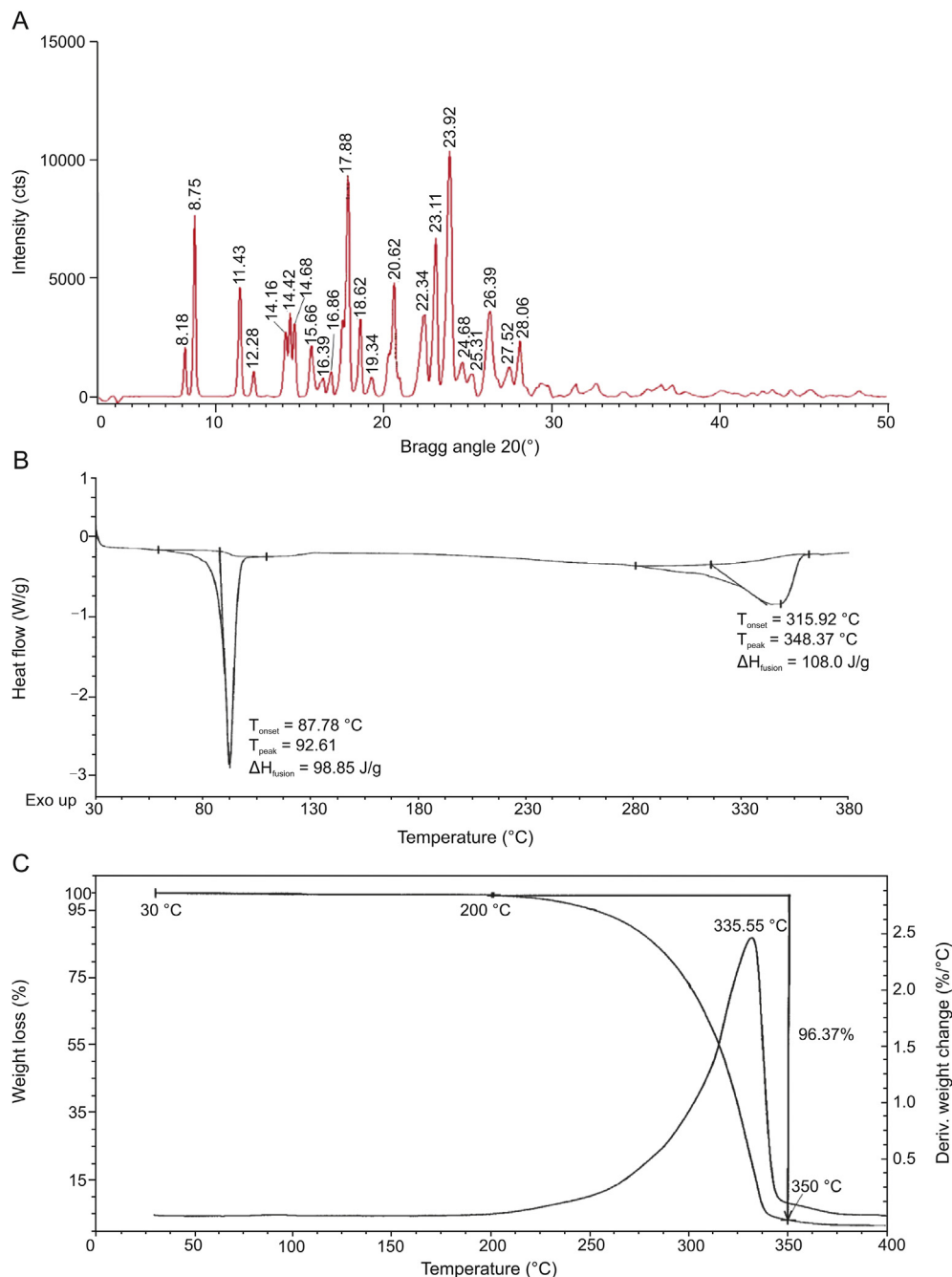
Fig. 4. (A) X-ray powder diffraction pattern, (B) DSC thermogram, and (C) TGA/DTG thermogram of THC.

3.3. Biological study of THC

3.3.1. In vitro cells viability by MTT assay

The effects of THC and CUR on cell proliferation of Hep G2, splenocytes, macrophages, and SH-SY5Y neuroblastoma cells were examined through MTT cell viability assay. The concentration-dependent increase in cell viability was observed till the tested THC and CUR concentrations. However, in various cell lines, the tested concentrations of THC and CUR resulted in cell viability more than 70% (Fig. S11, see the supplementary data).

3.3.2. Assessment of cytokines in splenocytes

The level of TNF-α was significantly (F [3,8] = 27.12, $P \leq 0.01$)

suppressed by 13.10% and 18.40% at 7.4 and 10 μg/mL, respectively, in the THC compared with the vehicle control. However, CUR suppressed the expression of TNF-α by 13.15% at 10 μg/mL, respectively, compared to vehicle control (Fig. 5A).

Literature reported that THC at 50 μM suppressed the 100 ng/mL LPS-stimulated TNF-α production and did not display a dose-dependent effect [29]. The current results revealed that THC suppressed TNF-α production in a dose-dependent manner. Further, THC showed a significant (F [3,8] = 25.65, $P \leq 0.01$) inhibition of IL-1β secretion by 31.60%, 41.81%, and 49.75% at 5, 7.4, and 10 μg/mL, respectively, as compared with the vehicle control group (Fig. 5B). Besides, CUR reduced the expression of IL-1β by 31.57% at 7.4 μg/mL compared to vehicle control. The level of MIP-1α was significantly

Table 2
X-ray powder diffraction data with Bragg angle, d-spacing, relative intensities, areas, and crystallite size of THC.

Bragg angle (°2θ)	FWHM[a] (°2θ)	Area (cts*°2θ)	d-spacing (Å)	Rel. Int.[b] (%)	Crystallite size (G, nm)
8.18	0.1535	377.18	10.81	24.56	28.75
8.75	0.1407	1070.42	10.11	76.03	31.38
11.43	0.2047	862.30	7.74	42.11	21.61
12.28	0.2430	224.81	7.21	9.24	18.22
14.16	0.1663	413.81	6.26	24.87	26.67
14.42	0.1151	403.58	6.14	35.04	38.55
14.68	0.1663	489.11	6.04	29.40	26.69
15.66	0.2047	419.80	5.66	20.50	21.71
16.39	0.1279	118.04	5.41	9.22	34.77
16.86	0.2814	265.95	5.26	9.45	15.81
17.88	0.2303	1970.55	4.96	85.54	19.35
18.62	0.1791	538.72	4.77	30.07	24.91
19.34	0.2047	129.40	4.59	6.32	21.81
20.62	0.1919	815.45	4.31	42.48	23.32
22.34	0.0900	360.49	3.98	29.62	49.86
23.11	0.1919	1252.24	3.85	65.23	23.41
23.92	0.1919	1919.83	3.72	100.00	23.45
24.68	0.1791	244.15	3.61	13.63	25.16
25.31	0.1535	184.73	3.52	12.03	29.39
26.39	0.2686	780.49	3.38	29.04	16.83
27.52	0.2814	332.49	3.24	11.81	16.11
28.06	0.1663	363.11	3.18	21.82	27.29

[a] Full width at half maximum.
[b] Relative intensity.

Table 3
Particle size distribution of magnesium gluconate.

Sample	d(0.1) (μm)	d(0.5) (μm)	d(0.9) (μm)	d(4,3) (μm)	SSA (m²/kg)
X$_1$	17.9	57.0	182.0	80.7	179.4
X$_2$	19.0	58.3	206.0	88.0	171.4
X$_3$	17.6	52.8	694.0	197.0	143.7
Average	18.2	56.0	360.7	121.9	164.8

(F [3,8] = 38.79, $P \leq 0.01$) inhibited by 8.24%, 9.75%, and 11.42% at 5, 7.4, and 10 μg/mL, respectively, in the THC group as compared to the vehicle control. MIP-1α was also significantly (F [3,8] = 175.65, $P \leq 0.01$) inhibited by 18.47% at 10 μg/mL in the CUR group as compared to the vehicle control.

3.3.3. Natural killer (NK) cells activity and phagocytosis

THC showed significant (F [3,8] = 50.58, $P \leq 0.001$) activation of NK cells activity by 36.97% and 44.54% at 5 and 10 μg/mL, respectively, compared to the vehicle control. In contrast, the NK cells activity was increased by 22.75% and 33.92% (F [3,8] = 21.68, $P \leq 0.05$) at 5 and 10 μg/mL, respectively, in the CUR group in relation to the vehicle control (Fig. 6A). The maximum percentage of phagocytosis in the THC and CUR groups was 115.96% and 111.54% (F [3,8] = 10.79, $P \leq 0.01$), respectively, at 1 μg/mL with respect to the vehicle control (Fig. 6B).

3.3.4. Anti-oxidation potential of THC

The level of LPO was significantly reduced in a dose-dependent manner, which indicated reduced oxidative damage to biomolecules suggesting the significant antioxidant potential of THC (Fig. 7) compared with CUR. LPO data showed a significant maximum decreased level by 68.57% (1.06 ± 0.03 μM; F [3,8] = 37.42, $P \leq 0.001$) by THC, while CUR showed only 7.73% decreased level of LPO at concentration of 10 μg/mL as compared with the vehicle control group, *i.e.*, H$_2$O$_2$ (20 mM) group (Fig. 7A). However, the level of SOD was significantly increased in a dose-dependent manner with the highest being 83.60% (F [3,8] = 48.35, $P \leq 0.001$), while CUR showed a maximum of 18.18% (F [3,8] = 35.27, $P \leq 0.01$) increase in

SOD level at 10 μg/mL as compared with the vehicle control, *i.e.*, H$_2$O$_2$ (20 mM) group (Fig. 7B). Besides, the level of CAT enzyme was increased by 63.02% (F [3,8] = 51.57, $P \leq 0.001$) in THC, while CUR showed the increased level by 26.63% at the concentration of 10 μg/mL as compared with the vehicle control, *i.e.*, H$_2$O$_2$ (20 mM) group (Fig. 7C). ABTS radical scavenging activity of THC and CUR was determined, which depicted the total antioxidant activity calculated from the decolorization of ABTS$^+$ spectrophotometrically. The result showed that different concentrations of THC and CUR had varying degree of scavenging potential for ABTS$^+$ radicals in a concentration-dependent manner (Fig. 7D). THC and CUR interaction suppressed the absorbance of the ABTS$^+$ radical cation, and the results are expressed as percentage inhibition. Maximum inhibition by 89.19% (F [3,8] = 17.52, $P \leq 0.001$), was reported at 1% THC concentration, while CUR showed 86.84% inhibition at 5% concentration.

3.3.5. Anti-oxidative damage and neuroprotective effects of THC

The results of THC and CUR against oxidative damage by hydrogen peroxide and neuroprotective action against MPP$^+$ induced neuronal damage are presented in Fig. 8. H$_2$O$_2$ (20 mM) decreased cell viability to 26.69%. In addition, THC significantly (F [3,8] = 32.81, $P \leq 0.001$) improved the cell viability to 52.80%, 66.90%, and 71.77% at tested concentrations of 0.1, 1, and 10 μg/mL, respectively, while CUR showed a maximum improved cell viability to 37.98% at 1 μg/mL (Fig. 8A).

Similarly, THC showed significant neuroprotective action against MPP$^+$. MPP$^+$ at 600 μM was used to induce neuronal damage. MPP$^+$ is toxic by interfering with the oxidative phosphorylation in mitochondria of the cells by inhibiting complex I, which leads to the depletion of ATP and results in cell death. The experimental data showed MPP$^+$ induced SH-SY5Y cell death and resulted in cell viability to 28.28%. However, THC at all the tested concentrations showed improved cell viability in a dose-dependent manner, but significant (F [3,8] = 24.17, $P \leq 0.001$) increase was found at 1 and 10 μg/mL to 43.97% and 58.60%, respectively (Fig. 8B). In contrast, CUR showed a maximum improved cell viability by 36.75% and 36.30% at 0.1 and 10 μg/mL, respectively.
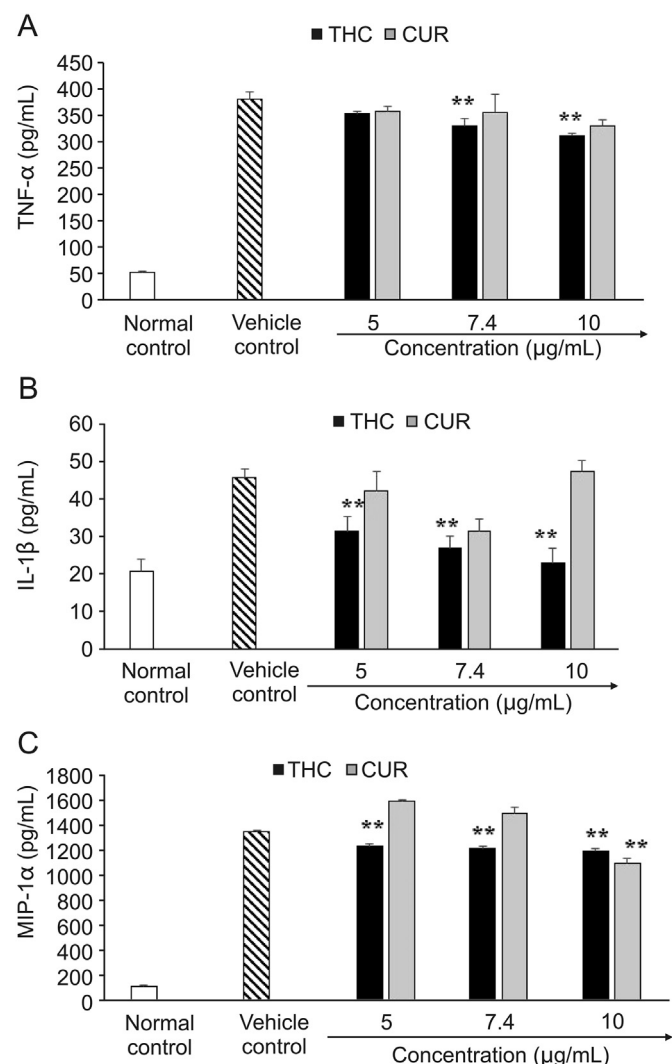
Fig. 5. Effect of THC and CUR on the cytokines expression in LPS induced mouse splenocytes. (A) TNF-α secretion, (B) IL-1β expression, and (C) MIP-1α. Data are expressed as mean $\pm$ SD, and represent the mean of three independent experiments ($n = 3$) using one-way ANOVA with Tukey's as a post hoc test *vs.* vehicle control. TNF-α $F[3,8] = 27.12$, **$P \leq 0.01$; IL-1β $F[3,8] = 25.65$, **$P \leq 0.01$; and MIP-1α $F[3,8] = 38.79$ for THC and $F[3,8] = 175.65$ for CUR, **$P \leq 0.01$.

4. Discussion

LC-MS analysis revealed the presence of THC in three different peaks at retention time of 16.08, 17.31, and 17.48 min with a distinguished behavior from other peaks. Now it was assumed that these 3 peaks represent the 3 forms of THC. Literature extensively studied the structure and properties of CUR. For example, CUR possibly can exist in nine possible conformations, i.e., two closed cis-enol forms, one open cis-enol form, three trans-enol forms, one cis-diketo form and two trans-diketo forms attributed to the presence of β-diketone functionality responsible for producing several interesting properties to CUR molecule both in the solid state and in solution [26]. Besides, CUR shows solid state polymorphism with three crystalline forms and one amorphous form [30,31]. X-ray crystal structure analysis revealed that CUR exists as keto-enol tautomers in the solid state. Extensive NMR study revealed that CUR in non-polar (CDCl$_3$) and polar aprotic solvents (DMSO-d_6) exists predominately as enolic form due to the intra-molecular hydrogen transfer; in the polar protic solvents like methanol, it exists as keto form [26,32]. Finally, LC-MS and NMR

studies confirmed that the enolic form of CUR is more stable in solution than keto form [7,33]. Like CUR, THC also exists in keto-enol form in solid state [5]. But there is no report about the existence of THC in keto-enol form in solution. Consequently, the FT-IR, proton, and carbon NMR analyses confirmed that our analyte existed in keto-enol form. Kawano et al. [33] demonstrated that the enolic form of CUR is the major form in solution (water/acetonitrile). Besides, CUR can exist in four enol conformations in DMSO [34]. Thus, it is assumed that peak at the retention time of 16.08 would be the keto form of THC, while peaks at the retention time of 17.31 and 17.48 min would be the two enol forms (1a and 1b) as shown in Fig. 1. However, further detailed studies using more advanced sensitive and sophisticated analytical techniques are required to design for finding out the actual structure for each peak as well as which structure, *i.e.,* 1a or 1b, will be the major form of THC.

Several literature reported XRPD, PSA, DSC, and TGA analyses of CUR [31,35,36]. Unfortunately, XRPD, PSA, DSC, and TGA analyses of THC are not reported anywhere according to the best of our knowledge. The XRPD analysis revealed that the analyte used for the study is crystalline in nature. This present result does not clearly indicate how many polymorphs exist in THC. But it might be advantageous to design for finding out different polymorphs of THC in the near future. DSC analysis demonstrated that the melting point of our commercially purchased THC was 92.61 °C, which is matched with reported value (m.p. 92–94 °C) [8]. TGA/DTG study revealed that THC exhibited the almost similar type of thermal degradation, but its thermal stability is higher than CUR [28,35,36]. This preliminary thermal study would be helpful in designing the kinetic study for THC degradation. Majeed and Badmaev [8] reported that their tetrahydrocurcuminoids were prepared by catalytical reduction of curcuminoids, produced from the turmeric followed by recrystallization and composed of 75%–85% THC, 10%–20% THDC, and 2.0%–4.5% THBDC. This tetrahydrocurcuminoids have the potential to regulate the physiological and pathological events in the skin and mucosa. The tetrahydrocurcuminoids used for the current study comprised 95.15% THC, 0.51% THDC, 0.94% OHC, and 3.40% HHC. Consequently, this analyte was used for biological activity, and its activities were compared with CUR. Our study shows that the three tautomeric structural forms of THC, namely, one keto and two enol forms, were observed in solution phase populations. The solution-phase structure of THC is also of great importance due to its biological and different pharmacological activities. Therefore, the isolation of these species and their quantitation will be useful from many perspectives as both these forms might show differences in biological activity. However, these tautomeric structures are to be verified experimentally. Crystal structures of these tautomeric forms of THC are not known. A combination of single X-ray crystallography, LC-NMR, ion mobility mass spectrometry (IM-MS), and theoretical calculations, including molecular docking, might be helpful in revealing the binding mode, amino acid interactions, and free binding energy of these tautomeric structures of THC.

Several studies compared various pharmacological activities of THC in both in vitro and in vivo models with respect to CUR. For example, THC exhibits higher activity than CUR in preventing DMH-induced ACF formation in mice and brain lipid peroxidation in diabetic rats, azoxymethane-induced colon carcinogenesis; inhibiting JNK activation, COX-dependent arachidonic acid metabolism [37]; suppressing radiation-induced lipid peroxidation, nitrilotriacetate-induced oxidative renal damage, LDL oxidation, and lipid peroxidation of erythrocyte membrane ghosts, carrageenin-induced inflammation; protecting from chloroquine-induced hepatotoxicity in rats; modulating renal and hepatic functional markers in diabetic rats; decreasing blood glucose and increasing plasma insulin in
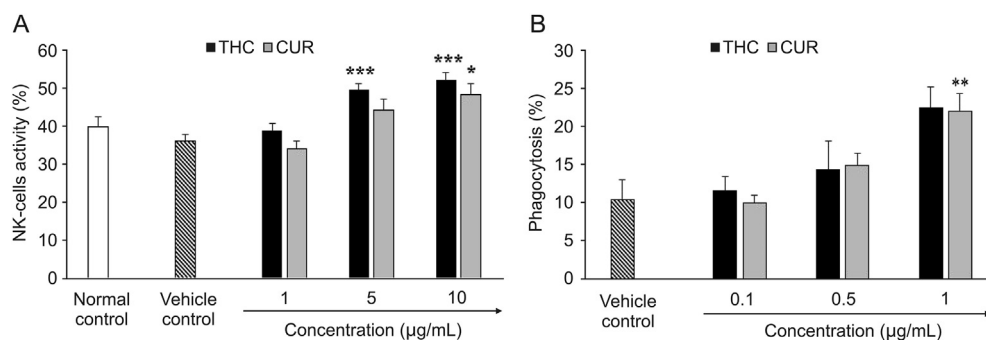
Fig. 6. Effect of THC and CUR on (A) Natural killer cells activity in LPS mediated splenocytes co-incubated with Yac-1 and (B) extent of phagocytosis in macrophages. Data are expressed as mean ± SD, and represent the mean of three independent experiments ($n = 3$) using one-way ANOVA with Tukey's as a post hoc test *vs.* vehicle control. NK cells F [3,8] = 50.58, ***$P \leq 0.001$ for THC and F [3,8] = 21.68 for CUR, *$P \leq 0.05$; and phagocytosis F [3,8] = 10.79, **$P \leq 0.01$.
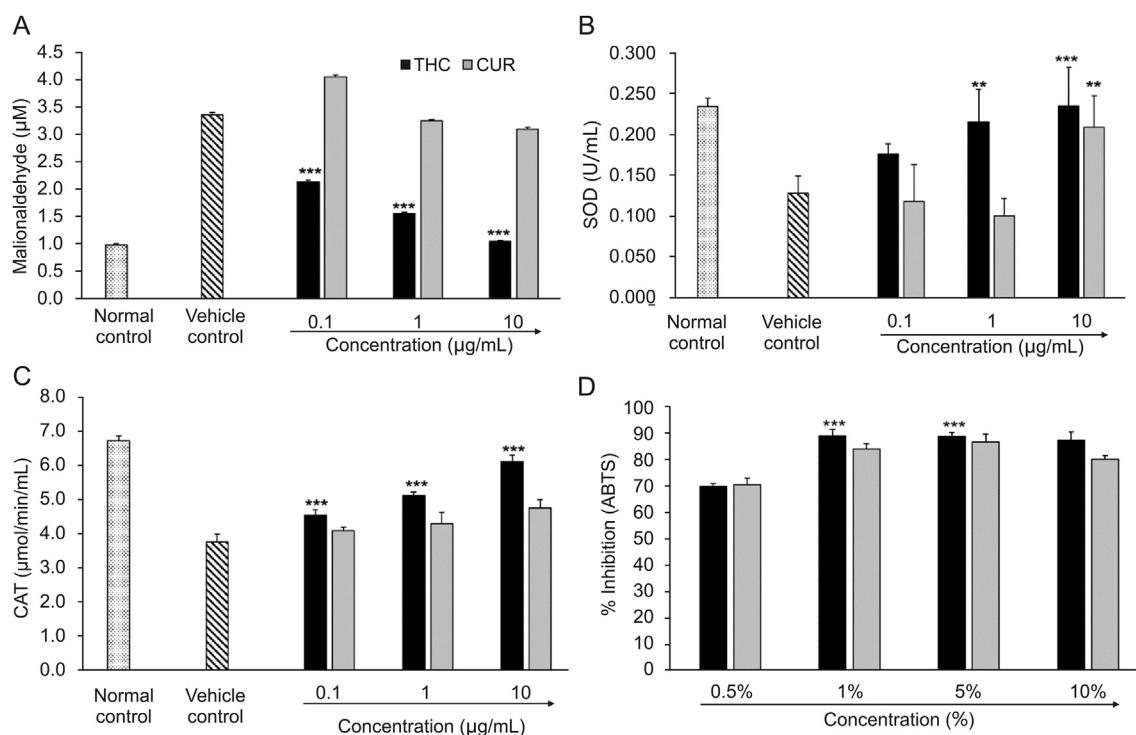

Fig. 7. Total antioxidant capacity of THC and CUR measured by (A) LPO, (B) SOD, (C) CAT, and (D) ABTS assay under standard reaction conditions. Data are expressed as mean ± SD, and represent the mean of three independent experiments ($n = 3$) using one-way ANOVA with Tukey's as a post hoc test *vs.* vehicle control. LPO F [3,8] = 37.42, ***$P \leq 0.001$; SOD F [3,8] = 48.35, ***$P \leq 0.001$ for THC and F [3,8] = 35.27, **$P \leq 0.01$ for CUR; CAT F [3,8] = 51.57, ***$P \leq 0.001$; and ABTS F [3,8] = 17.52, ***$P \leq 0.001$.

diabetic rats; increasing tissue sialic acid; reducing accumulation and cross-linkage of collagen in diabetic rats; a hepatoprotective role in CCl$_4$-induced liver damage in rats and alcoholic liver disease model rats; improving the specific insulin binding to the receptors on erythrocytes; binding to phospholipase 2, an antihypertensive; activating p53 and p21. THC is less active than CUR in inhibiting the activity of 5-LOX; preventing PMA-induced skin tumor promotion in mice; suppressing NF-kB activation; modulation of ABC drug transporters; inhibiting the Wnt/beta-catenin pathway by decreasing the amount of the transcriptional coactivator p300; reducing β-amyloid and phosphorylated Tau protein burden in Alzheimer transgenic mice; suppressing LPS-induced production of TNF-α; inhibiting TNF-induced expression of cyclin D1 and VEGF.

THC does not induce ROS production and membrane mobility co-efficient or show any pro-oxidant activity [4,9,11]. Proinflammatory cytokines like TNF-α, IL-1β, and MIP-1α play a vital role in the pathogenesis of immune, inflammation, cardiovascular diseases, cancer, and neurodegenerational disease through a series of cytokine signaling pathways. Our tetrahydrocurcuminoids showed higher activity than CUR in the reduction of the LPS-induced over-expressions of TNF-α, IL-1β, and MIP-1α in a dose-dependent manner in the mouse splenocyte cells. Lipid peroxidation has been involved in several disease states such as atherosclerosis, IBD, ROP, BPD, asthma, Parkinson's disease, kidney damage, and preeclampsia [38]. Literature reported the superior anti-oxidant activities of THC than CUR in various in vitro and in vivo models. Turmeric reduces
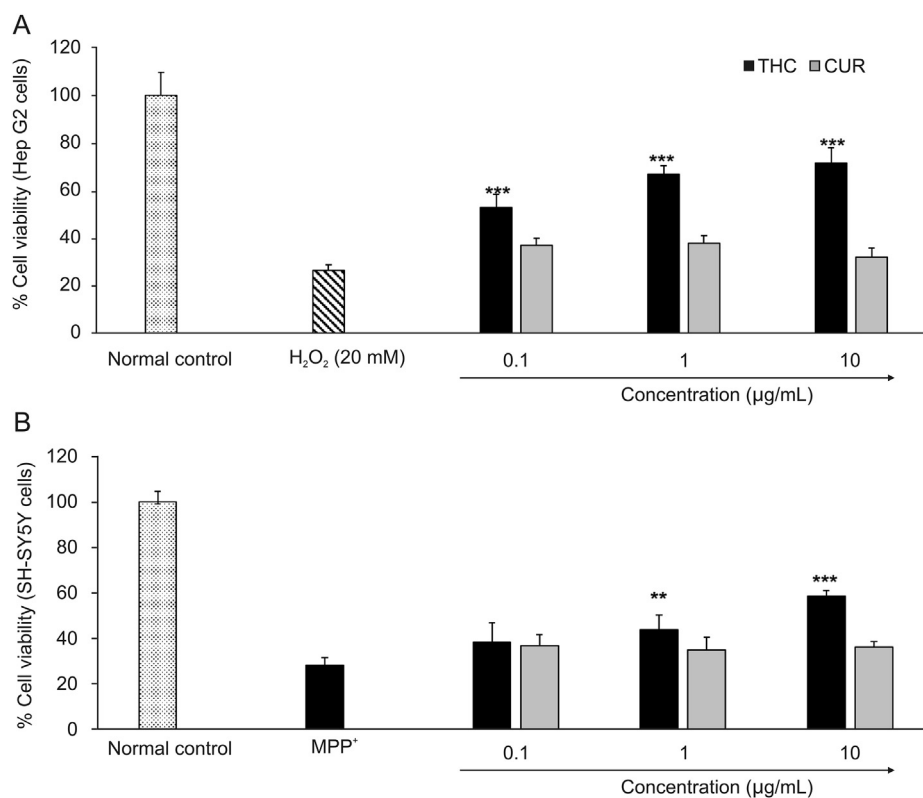
Fig. 8. Evaluation of THC and CUR (A) defense against oxidative stress and (B) neuroprotective action. Data are expressed as mean $\pm$ SD, and represent the mean of three independent experiments ($n = 3$) using one-way ANOVA with Tukey's as a post hoc test *vs.* vehicle control. Defense against oxidative stress/neuroprotective action F [3,8] $= 32.81$ for H_2O_2 and F [3,8] $= 24.17$ for MPP$^+$, ***$P \leq 0.001$.

lipid peroxidation by increasing the activities of antioxidant enzymes, i.e., superoxide dismutase (SOD), catalase (CAT), and glutathione peroxidase (GPx). THC showed a significant inhibitory effect on lipid peroxidation in different models as compared with CUR [4,9,11]. The present study revealed that THC significantly ($P \leq 0.001$) reduced the hydrogen peroxide induced lipid peroxidation (LPO) in a dose-dependent manner. However, the level of LPO was significant reduction as compared with that of CUR. Similarly, SOD and CAT levels were significantly ($P \leq 0.001$) improved in the THC group in a dose-dependent manner, while the results were significantly high as compared with those of CUR. ABTS radical scavenging activity of THC and CUR was determined, which depicted the total antioxidant activity and was calculated from the decolorization of ABTS$^+$ spectrophotometrically as ABTS$^+$ is a blue chromophore produced by the reaction between ABTS and potassium persulfate. THC and CUR while addition to preformed radical cation (ABTS$^+$), reduced it to ABTS. The result showed that different concentrations of THC and CUR showed varying degree of scavenging potential for ABTS$^+$ radicals in a concentration-dependent manner (Fig. 7D). However, THC suppressed the absorbance of the ABTS$^+$ radical cation with higher rates compared with CUR, and the results are expressed as percentage inhibition. Wu et al. [2] demonstrated that THC protected from oxidative damage and neurodegenerative disorder in different in vitro and in vivo models. THC exhibited significant ($P \leq 0.001$) improved cell viability against hydrogen peroxide induced Hep G2 cells, indicating that THC protects against the oxidative stress induced cell damage, and the results are comparable with those of CUR. Besides, THC exhibited significant ($P \leq 0.001$) improved cell viability against MPP$^+$ induced SH-SY5Y cells, indicating that THC possesses significant neuroprotective activity compared with CUR. THC has been shown different activities potential against cancer cell lines in different

models compared with CUR [39]. It is assumed that the purity of THC, composition of THC and the keto-enol form might affect the biological activity of THC.

5. Conclusions

The comprehensive characterization of tetrahydrocurcuminoids using advanced spectroscopic and thermoanalytical techniques revealed the existence of the keto-enol form of THC in both solid and liquid states. Besides, the present sample was a mixture of THC, THDC, HHC, and OHC, which has a different composition from that of reported tetrahydrocurcuminoids. THC was found to be thermally more stable than CUR. THC in our tetrahyrdocurcuminoids for first time was observed to be present in three different conformations/forms *viz.* one keto form and two enol forms (1a and 1b). LC-MS, NMR, and FT-IR analyses indicated that the enol form was the major and more stable form of THC. Further detailed studies using advanced, sophisticated analytical techniques like NMR crystallography, LC-NMR, and 2D NMR, might be helpful in identifying each form of THC accurately. The present tetrahyrdocurcuminoids exhibited significant suppression of proinflammatory cytokines, increased NK cells and phagocytosis activities, higher total antioxidant activity, protection from the oxidative stress induced cell damage, and neuroprotective activity compared with CUR in a concentration-dependent fashion. The variation of the biological activities of a pharmaceutical/nutraceutical solely depends on its active form and presence of other impurities. As the chemistry of THC is more complicated, and there may be different keto-enol forms and analogs, it is essential to conduct full characterization in both solid and liquid states before performing the biological activities. Thus, the authors conclude that the present study would be helpful in designing a research plan on THC for better understanding

its physicochemical properties and biological variation.

Conflicts of interest

The authors declare that there are no conflicts of interest.

Acknowledgments

Appendix A. Supplementary data

Supplementary data to this article can be found online at https://doi.org/10.1016/j.jpha.2020.02.005.

References

[1] A. Hassaninasab, Y. Hashimoto, K. Tomita-Yokotani, et al., Discovery of the curcumin metabolic pathway involving a unique enzyme in an intestinal microorganism, Proc. Natl. Acad. Sci. U. S. A 108 (2011) 6615—6620.

[2] J.C. Wu, M.L. Tsai, C.S. Lai, et al., Chemopreventative effects of tetrahydrocurcumin on human diseases, Food Funct 5 (2014) 12—17.

[3] K. Bairwa, J. Grover, M. Kania, et al., Recent developments in chemistry and biology of curcumin analogues, RSC Adv. 4 (2014) 13946—13978.

[4] P. Anand, S.G. Thomas, A.B. Kunnumakkara, et al., Biological activities of curcumin and its analogues (Congeners) made by man and mother nature, Biochem. Pharmacol. 76 (2008) 1590—1611.

[5] C.R. Girija, N.S. Begum, A.A. Syed, et al., Hydrogen-bonding and C-H…π interactions in 1,7-bis(4-hydroxy-3-methoxyphenyl)heptane-3,5- dione (tetrahydrocurcumin), Acta Crystallogr. C 60 (2004) o611—o613.

[6] P. Limtrakul, W. Chearwae, S. Shukla, et al., Modulation of function of three ABC drug transporters, P-glycoprotein (ABCB1), mitoxantrone resistance protein (ABCG2) and multidrug resistance protein 1 (ABCC1) by tetrahydrocurcumin, a major metabolite of curcumin, Mol. Cell. Biochem. 296 (2007) 85—95.

[7] S.I. Hoehle, E. Pfeiffer, A.M. Sólyom, et al., Metabolism of curcuminoids in tissue slices and subcellular fractions from rat liver, J. Agric. Food Chem. 54 (2006) 756—764.

[8] M. Majeed, V. Badmaev, Use of Tetrahydrocurcuminoids to Regulate Physiological and Pathological Events in the Skin and Mucosa, US patent, WO2000061162 A9, 2001.

[9] B.B. Aggarwal, L. Deb, S. Prasad, Curcumin differs from tetrahydrocurcumin for molecular targets, signaling pathways and cellular responses, Molecules 20 (2015) 185—205.

[10] S. Park, L.R. Lee, J.H. Seo, et al., Curcumin and tetrahydrocurcumin both prevent osteoarthritis symptoms and decrease the expressions of proinflammatory cytokines in estrogen-deficient rats, Genes Nutr. 11 (2016) 2.

[11] The molecular targets and therapeutic uses of curcumin in health and disease, in: B.B. Aggarwal, Y.-J. Surh, S. Shishodia (Eds.), Advances in Experimental Medicine and Biology, vol. 595, Springer International Publishing, Switzerland, 2007, pp. 490.

[12] M.K. Trivedi, M. Gangwar, S.C. Mondal, et al., Protective effects of tetrahydrocurcumin (THC) on fibroblast and melanoma cell lines *in vitro*: it's implication for wound healing, J. Food Sci. Technol. 54 (2017) 1137—1145.

[13] D.A.T. Pires, W.L. Pereira, R.R. Teixeira, et al., Nuclear magnetic resonance (NMR), infrared (IR) and mass spectrometry (MS) study of keto-enol tautomerism of isobenzofuran-1(3H)-one derivatives, J. Mol. Struct. 1113 (2016) 146—152.

[14] P.J. Taylor, G. van der Zwan, L. Antonov, Tautomerism: introduction, history, and recent developments in experimental and theoretical methods, in: L. Antonov (Ed.), Tautomerism: Methods and Theories, 1st ed., Wiley-VCH Verlag GmbH & Co. KGaA, 2014.

[15] M.K. Trivedi, P. Panda, K.K. Sethi, et al., Metabolite profiling in *Withania somnifera* roots hydroalcoholic extract using LC/MS, GC/MS and NMR spectroscopy, Chem. Biodivers. 14 (2017) e1600280.

[16] M.K. Trivedi, N. Dixit, K.K. Sethi, et al., In-depth investigation on physicochemical and thermal properties of magnesium (II) gluconate using spectroscopic and thermoanalytical techniques, J. Pharma. Anal. 7 (2017) 332—337.

[17] M.K. Trivedi, S.C. Mondal, M. Gangwar, et al., Effect of a novel ashwagandha-based herbomineral formulation on pro-inflammatory cytokines expression in mouse splenocyte cells: a potential immunomodulator, Phcog. Mag. 13 (2017) 90—94.

[18] J. Małaczewska, The splenocyte proliferative response and cytokine secretion in mice after 28-day oral administration of silver nanocolloid, Pol. J. Vet. Sci. 17 (2014) 27—35.

[19] M. Berridge, A. Tan, K. McCoy, et al., The biochemical and cellular basis of cell proliferation assays that use tetrazolium salts, Biochemica 4 (1996) 14—19.

[20] G.C. Keustermans, S.B. Hoeks, J.M. Meerding, et al., Cytokine assays: an assessment of the preparation and treatment of blood and tissue samples, Methods 61 (2013) 10—17.

[21] S.B. Lee, J. Cha, I.K. Kim, et al., A high-throughput assay of NK cell activity in whole blood and its clinical application, Biochem. Biophys. Res. Commun. 445 (2014) 584—590.

[22] S.J. Gebran, E.L. Romano, H.A. Pons, et al., A modified colorimetric method for the measurement of phagocytosis and antibody-dependent cell cytotoxicity using 2,7-diaminofluorene, J. Immunol. Methods 151 (1992) 255—260.

[23] R. Re, N. Pellegrini, A. Proteggente, et al., Antioxidant activity applying an improved ABTS radical cation decolorization assay, Free Radic. Biol. Med. 26 (1999) 1231—1237.

[24] R.J. Ruch, S.J. Cheng, J.E. Klaunig, Prevention of cytotoxicity and inhibition of intercellular communication by antioxidant catechins isolated from Chinese green tea, Carcinogenesis 10 (1989) 1003—1008.

[25] C. Shen, W. Xian, H. Zhou, et al., Potential protective effects of autophagy activated in MPP^+ treated astrocytes, Exp. Ther. Med. 12 (2016) 2803—2810.

[26] K.I. Priyadarsini, Photophysics, photochemistry and photobiology of curcumin: studies from organic solutions, bio-mimetics and living cells, J. Photochem. Photobiol. C Photochem. Rev. 10 (2009) 81—95.

[27] J.I. Langford, A.J.C. Wilson, Scherrer after sixty years: a survey and some new results in the determination of crystallite size, J. Appl. Crystallogr. 11 (1978) 102—113.

[28] F. Jasim, T. Talib, Some observations on the thermal behavior of curcumin under air and argon atmospheres, J. Therm. Anal. 38 (1992) 2549—2552.

[29] M. Nishida, S. Nishiumi, Y. Mizushina, et al., Monoacetyl-curcumin strongly regulates inflammatory responses through inhibition of NF-κB activation, Int. J. Mol. Med. 25 (2010) 761—767.

[30] G. Grynkiewicz, P. Ślifirski, Curcumin and curcuminoids in quest for medicinal status, Acta Biochim. Pol. 59 (2012) 201—212.

[31] M.L.A.D. Lestari, G. Indrayanto, Curcumin, in: H.G. Brittain (Ed.), Profiles of Drug Substances, Excipients, and Related Methodology, vol 39, Academic Press, Burlington, 2014, ppp. 113—204.

[32] F. Payton, P. Sandusky, W.L. Alworth, NMR study of the solution structure of curcumin, J. Nat. Prod. 70 (2007) 143—146.

[33] S.-I. Kawano, Y. Inohana, Y. Hashi, et al., Analysis of keto-enol tautomers of curcumin by liquid chromatography/mass Spectrometry, Chin. Chem. Lett. 24 (2013) 685—687.

[34] C.A. Slabber, C.D. Grimmer, R.S. Robinson, Solution conformations of curcumin in DMSO, J. Nat. Prod. 79 (2016) 2726—2730.

[35] Z. Zhao, M. Xie, Y. Li, et al., Formation of curcumin nanoparticles *via* solution-enhanced dispersion by supercritical CO_2, Int. J. Nanomed. 10 (2015) 3171—3181.

[36] Z. Chen, Y. Xia, S. Liao, et al., Thermal degradation kinetics study of curcumin with nonlinear methods, Food Chem. 155 (2014) 81—86.

[37] C.S. Lai, J.C. Wu, S.F. Yu, et al., Tetrahydrocurcumin is more effective than curcumin in preventing azoxymethane-induced colon carcinogenesis, Mol. Nutr. Food Res. 55 (2011) 1819—1828.

[38] C. Mylonas, D. Kouretas, Lipid peroxidation and tissue damage, In Vivo 13 (1999) 295—309.

[39] P. Yoysungnoen, P. Wirachwong, C. Changtam, et al., Anti-cancer and anti-angiogenic effects of curcumin and tetrahydrocurcumin on implanted hepatocellular carcinoma in nude mice, World J. Gastroenterol. 14 (2008) 2003—2009.